

Line-driven disk wind models with an improved line force

Daniel Proga^{a,b}, James M. Stone^c, and Janet E. Drew^a

^a Imperial College of Science, Technology and Medicine, Blackett Laboratory, Prince Consort Road, London SW7 2BZ, UK

^b new address Laboratory for High Energy Astrophysics, NASA Goddard Space Flight Center, Greenbelt, MD 20771, USA

^c Department of Astronomy, University of Maryland, College Park MD 20742, USA

E-mail: *d.proga@ic.ac.uk*, *jstone@astro.umd.edu*, and *j.drew@ic.ac.uk*

28 December 2017

ABSTRACT

We describe an efficient method of calculating the radiation pressure due to spectral lines, including all the terms in the velocity gradient tensor. We apply this method to calculate the two-dimensional, time-dependent structure of winds from luminous disks. Qualitative features of our new models are very similar to those we calculated including only the dominant terms in the tensor (Proga, Stone & Drew 1998, hereafter PSD). In particular, we find that models which displayed unsteady behaviour in PSD are also unsteady with the new method, and gross properties of the winds, such as mass-loss rate and characteristic velocity are not changed by the more accurate approach. The largest change caused by the new method is in the disk-wind opening angle: winds driven only by the disk radiation are more polar with the new method while winds driven by the disk and central object radiation are typically more equatorial. In the closing discussion, we provide further insight into the way the geometry of the radiation field and consequent flow determines the time properties of the flow.

Key words: accretion discs – hydrodynamics – methods: numerical – stars: mass-loss – stars: early-type – galaxies: nuclei

1 INTRODUCTION

There has long been an awareness that radiation pressure due to spectral lines should be capable of driving winds from luminous disks (e.g., Vitello & Shlosman 1988, Murray et al. 1995). However, the geometry of the case demands a multi-dimensional treatment that has only recently been undertaken by Pereyra, Kallman & Blondin 1997) and ourselves (Proga, Stone & Drew 1998, hereafter PSD). A surprising outcome of our models was that, in cases where the driving radiation field is dominated by the contribution from the disk, the flow is unsteady. Despite the complex structure of the disk wind in this case, the time-averaged mass loss rate and terminal velocity fit onto the same scaling with luminosity as do steady flows obtained where the radiation is dominated by the central object. In fact these relations have been shown to be similar to those well-established by analysis for spherically-symmetric stellar winds (Proga 1999).

Our models adopt the method for calculating the line acceleration for one-dimensional radial flows, first introduced by Castor, Abbott & Klein (1975, hereafter CAK), that has since been further developed within the context of stellar winds from hot, luminous OB stars (Friend & Abbott 1986; Pauldrach, Puls & Kudritzki 1986). In order to

extend the CAK method to describe multi-dimensional disk winds, it is necessary to accommodate the effects of the three-dimensional velocity field and the direction-dependent intensity. These effects can lead to qualitatively different results compared to those obtained from a one-dimensional treatment (see, for example, Owocki, Cranmer & Gayley, 1996, hereafter OCG, on the case of a rapidly rotating star).

The most difficult aspect of calculating the line force in a disk wind is in the evaluation of the integral involving the velocity gradient tensor (Q , which controls the anisotropic line opacity) over the entire solid angle occupied by radiating surfaces. In our previous models, we followed the example of Icke's (1980) earlier numerical work on disk winds driven by continuum radiation pressure. In this approach, the integral was evaluated using an angle-adaptive quadrature to ensure an accurate result. However, computational limitations required that we simplify the integrand, retaining only the dominant terms in the velocity gradient tensor. Specifically, we kept only the radial gradient in the evaluation of the acceleration due to the radiation from the central object, and the vertical gradient for the acceleration due to the disk. Moreover, we dropped azimuthal terms that are present in a rotating flow. In this paper, we introduce a new quadrature that avoids any simplification of the integrand. This allows us to evaluate the radiation force for completely arbitrary

velocity fields within the context of the CAK formalism. We can now explore the consequences of the approximations in our previous work and move onto a more general formulation.

In this paper we recalculate several disk wind models first presented in PSD. We concentrate on assessing how gross properties – such as the mass-loss rate, velocity, opening angle and time behaviour of disk winds – change when Q , the velocity gradient tensor, is treated in full. We describe our ‘full-Q’ method for a general three dimensional case in Section 2. Our new method of numerical evaluation of the line force is described in Section 3. We show our new results and compare them with those in PSD in Section 4, and discuss the implications in Section 5.

2 METHOD

To compute the structure and evolution of a line-driven wind from a luminous disk, we solve the equations of hydrodynamics

$$\frac{D\rho}{Dt} + \rho \nabla \cdot \mathbf{v} = 0, \quad (1)$$

$$\rho \frac{D\mathbf{v}}{Dt} = -\nabla(\rho c_s^2) + \rho \mathbf{g} + \rho \mathbf{F}^{rad} \quad (2)$$

where ρ is the mass density, \mathbf{v} the velocity, \mathbf{g} the gravitational acceleration of the central star, and \mathbf{F}^{rad} the total radiation force per unit mass. The gas in the wind is taken to be isothermal with a sound speed c_s .

We adopt the same geometry and assumptions to compute the radiation field from the disk and central star as in PSD. That is, we consider the disk to be flat, Keplerian, geometrically-thin and optically-thick. The radiation field of the disk is specified by assuming that the temperature follows the radial profile of the so-called α -disk (Shakura & Sunyaev 1973), and therefore depends only on the mass accretion rate in the disk, \dot{M}_a , and the mass and radius of the central star, M_* and r_* . In models where the central star is also radiant, we take into account the stellar irradiation of the disk, assuming that the disk re-emits all absorbed energy locally and isotropically. See PSD and below for further details.

As in PSD, we approximate the radiative acceleration due to lines (line force, for short) using a modified CAK method. The line force at a point W defined by the position vector \mathbf{r} is

$$\mathbf{F}^{rad,l}(\mathbf{r}) = \oint_{\Omega} M(t) \left(\hat{n} \frac{\sigma_e I(\mathbf{r}, \hat{n}) d\Omega}{c} \right) \quad (3)$$

where I is the frequency-integrated continuum intensity in the direction defined by the unit vector \hat{n} , and Ω is the solid angle subtended by the disk and star at the point W. The term in brackets is the electron-scattering radiation force, σ_e is the mass-scattering coefficient for free electrons, and $M(t)$ is the force multiplier – the numerical factor which parameterises by how much spectral lines increase the scattering coefficient. In the Sobolev approximation, $M(t)$ is a function of the optical depth parameter

$$t = \frac{\sigma_e \rho v_{th}}{|dv_l/dl|}, \quad (4)$$

where v_{th} is the thermal velocity, and $\frac{dv_l}{dl}$ is the velocity gradient along the line of sight.

We adopt the CAK analytical expression for the force multiplier as modified by Owocki, Castor & Rybicki (1988, see also PSD)

$$M(t) = kt^{-\alpha} \left[\frac{(1 + \tau_{max})^{(1-\alpha)} - 1}{\tau_{max}^{(1-\alpha)}} \right] \quad (5)$$

where k is proportional to the total number of lines, α is the ratio of optically thick to optically-thin lines, $\tau_{max} = t\eta_{max}$ and η_{max} is a parameter related to the opacity of the most optically thick lines. The term in the square brackets is the Owocki, Castor & Rybicki correction for the saturation of $M(t)$ as the wind becomes optically thin even in the strongest lines, i.e.,

$$\lim_{\tau_{max} \rightarrow 0} M(t) = M_{max} = k(1 - \alpha)\eta_{max}^{\alpha}.$$

In the generalized Sobolev method $\frac{dv_l}{dl}$ may be written as $\frac{dv_l}{dl} = \hat{n} \cdot \nabla(\hat{n} \cdot \mathbf{v})$, or as in Rybicki & Hummer (1978) (see also PSD)

$$\frac{dv_l}{dl} = Q \equiv \sum_{i,j} \frac{1}{2} \left(\frac{\partial v_i}{\partial r_j} + \frac{\partial v_j}{\partial r_i} \right) n_i n_j = \sum_{i,j} e_{ij} n_i n_j \quad (6)$$

where e_{ij} is the symmetric rate-of-strain tensor, and v_i , r_i , and n_i are the components of \mathbf{v} , \mathbf{r} , and \hat{n} respectively. In the generalized 3D case, the flow velocity along \hat{n} may not be monotonic, resulting in radiative coupling between distant parts of the flow and making t a non local quantity. Here we do not take into account the non local effects on t but rather concentrate on taking into account all terms of Q .

As in PSD, we use the ZEUS-2D code to numerically integrate the hydrodynamical equations 1 and 2. We describe our numerical algorithm for evaluating the line force in the next section. For a rotating flow, there may be an azimuthal component to the line force even in axisymmetry. In contrast to the approximate method used in PSD, the

full-Q formulation used here allows us to treat the effects of a non-zero azimuthal component to the radiation force on the wind self-consistently. We examine these effects in detail in section 4.

3 NUMERICAL EVALUATION OF THE LINE FORCE

The disk line force is a complicated integral in which the dependences on geometry, the radiation field and local optical depth are not separable. In practice, this integral must be evaluated over the whole computational domain at every time step of the hydrodynamical calculations. A fast numerical integration scheme is therefore essential.

We perform our calculations in spherical polar coordinates (r, θ, ϕ) with $r = 0$ at point C, the center of the central star. We measure colatitude, θ , from the rotation axis of the disk and assume axial symmetry about this axis. Azimuth, ϕ , is measured from a plane perpendicular to the disk plane, containing the point C and a point W above the disk. We define the position of a wind point, W, and of a disk point, D, by the vectors $\mathbf{r} = (r, \theta, \phi = 0^\circ)$ and $\mathbf{r}_D = (r_D, \theta_D = 90^\circ, \phi_D)$, respectively.

To specify directions \hat{n} about W we use a second spherical polar coordinate system which has an origin at W, colatitude, θ_1 , measured from the direction C toward W, and azimuth, ϕ_1 , measured from a plane perpendicular to the disk plane, and containing C and W. The components of \hat{n} in the (r, θ, ϕ) system expressed in terms of θ_1 and ϕ_1 are

$$\hat{n} = (n_r, n_\theta, n_\phi) = (\cos \theta_1, \sin \theta_1 \cos \phi_1, \sin \theta_1 \sin \phi_1). \quad (7)$$

and an element of the solid angle is

$$d\Omega = \sin \theta_1 d\theta_1 d\phi_1. \quad (8)$$

Note the transformation between this second coordinate system (on which we evaluate the radiative acceleration) and the original (which defines the hydrodynamical grid) is a combination of a displacement of the origin by \mathbf{r} and rotation by θ .

In the disk plane at $r = r_D$, $I(\mathbf{r}, \hat{n})$ is the local isotropic disk intensity:

$$I_D(r_D) = \frac{3GM_*\dot{M}_a}{8\pi^2r_*^3} \left\{ \frac{r_*^3}{r_D^3} \left(1 - \left(\frac{r_*}{r_D} \right)^{1/2} \right) + \frac{x}{3\pi} \left(\arcsin \frac{r_*}{r_D} - \frac{r_*}{r_D} \left(1 - \left(\frac{r_*}{r_D} \right)^2 \right)^{1/2} \right) \right\}, \quad (9)$$

We include the effects of the irradiation of a disk by a star for $x > 0$ where x is defined as the ratio between the stellar

luminosity L_* and the disk luminosity, L_D (PSD). The coordinates of \mathbf{r}_D in the system defining the hydrodynamical grid, expressed in the second coordinate system centered on W, are:

$$r_D = (r^2 + d_D^2 - 2rd_D \cos \theta_1)^{1/2} \quad (10)$$

$$\theta_D = 90^\circ \quad (11)$$

$$\phi_D = \arcsin \frac{d_D \sin \theta_1 \sin \phi_1}{(r^2 + d_D^2 - 2rd_D \cos \theta_1)^{1/2}} \quad (12)$$

where $d_D = r \cos \theta / (\cos \theta \cos \theta_1 - \sin \theta \sin \theta_1 \cos \phi_1)$ is the distance between D and W. For radiation from the star, the intensity may be written:

$$I_* = \frac{L_*}{4\pi^2 r_*^2} = x \frac{GM_* \dot{M}_a}{8\pi^2 r_*^3}. \quad (13)$$

The precise location on the star of the point of emission is not relevant because we assume that the stellar surface is isothermal.

We split the integration of the line force over Ω (see eq. 3) into the integration over the stellar solid angle, Ω_* and the disc solid angle, Ω_D . We take into account the effects due to shadowing of the disk by the star, and occultation of the star by the disk, by properly defining the limits of integration for each. The contributions to the line force due to the disk and star are respectively

$$\mathbf{F}_D^{rad,e} = \oint_{\Omega_D} M(t) \left(\hat{n} \frac{\sigma_e I_D d\Omega}{c} \right) \quad (14)$$

and

$$\mathbf{F}_*^{rad,e} = \oint_{\Omega_*} M(t) \left(\hat{n} \frac{\sigma_e I_* d\Omega}{c} \right). \quad (15)$$

The actual variables we use in the integration are μ and ϕ_1 for the radial line force, μ and ν_s for the latitudinal line force, and μ and ν_c for the azimuthal line force, where $\mu = \cos \theta_1$, $\nu_s = \sin \phi_1$ and $\nu_c = \cos \phi_1$. Using these new variables we can write $\hat{n} d\Omega$ in eqs (14) and (15) as

$$\hat{n} d\Omega = (-\mu d\mu d\phi_1, -\sqrt{1-\mu^2} d\mu d\nu_s, \sqrt{1-\mu^2} d\mu d\nu_c). \quad (16)$$

Note the force multiplier $M(t)$ in equations 14 and 15 depends on the rate of strain tensor e_{ij} via equations 4 through 6. The components of this tensor in spherical polar coordinates are given, e.g., in Batchelor (1967). We evaluate these from the velocity components on the hydrodynamical grid by using finite-difference approximations to the terms in e_{ij} . The ZEUS-2D code uses a staggered grid such that scalars and the components of vectors and tensors are centered at different locations on the grid. For example, discrete values for the density are stored at zone centers, v_r values are stored at zone interfaces in the radial direction, and v_θ components

are stored at zone interfaces in the latitudinal direction (see Stone & Norman 1992 for details). Subsequently different components of the line force (and therefore corresponding $M(t)$ and e_{ij}) are also defined at different locations on the grid. To properly evaluate e_{ij} at a given location we have to calculate discrete values of the appropriate variables at, and variable differences around, this location. We take simple means of variable pairs if we need to calculate a value mid-way between hydrodynamic grid points.

We apply the trapezoidal method to integrate the line force due to both the star and disk. We find that a dozen quadrature points for μ and for ϕ_1 (or ν_s or ν_c) are sufficient to achieve a satisfactory accuracy of the disk and stellar line force even for W near the disk plane and stellar surface. This represents a considerable reduction in the number of quadrature points compared to the original discretization of solid angle used in PSD. This reduction is possible because of the simple form of the $\hat{n}d\Omega$ factor (see eq. 16) in the full-Q method used here in comparison to the method implemented in PSD. For example, in the disk contribution to the radial component of the line force, we here have $n_r d\Omega = -\mu d\mu d\phi_1$ as compared with the form in PSD:

$$n_r d\Omega = \frac{r - r_D \sin \theta \cos \phi_D}{d_D} \frac{r \cos \theta}{d_D^3} r_D dr_D d\phi_D \quad (17)$$

where $d_D = (r_D^2 + r^2 - 2r_D r \sin \theta \cos \phi_D)^{1/2}$ (see Appendix A in PSD).

To ensure proper cancellation of the contributions to the net value of the line force from regions of the disk corresponding to negative (positive) n_r , we break the integration over μ into sub-intervals for negative (positive) μ . Similarly, we break the integration over ϕ_1 into sub-intervals for negative (positive) ϕ_1 , corresponding to negative (positive) intervals for both ν_s or ν_c .

To afford a full recalculation of the line force for all locations at every time step we need not only a relatively low number of quadrature points, but also a short computational time per quadrature point. We reduce the latter by computing all the terms in brackets in eqs 14 and 15 at the beginning of each model, as they depend only on the radiation field geometry. We then use these precalculated factors throughout the time evolution. Thus, to evaluate eqs 14 and 15 at every hydrodynamical grid point and every time step, we have to (i) calculate $M(t)$, (ii) multiply it by the precalculated geometric factors for all quadrature points (12^2 in this case), and (iii) sum up the products. The price to pay for this reduction in computation is an increase in memory because we have to store all pre-calculated geometric factors for all grid points, quadrature points and line force components.

4 RESULTS

4.1 Comparison between new and previous models

Using our new ‘full-Q’ method to compute the line force, we have recomputed five models using the same parameters as runs 2, 3, 8, 12 and 14 in PSD. This range of models illustrates the dependence of the disk wind on the disk and stellar luminosity. Table 1 summarises the gross properties of our new calculations in comparison to PSD including the mass-loss rate, \dot{M}_w , characteristic velocity at $10r_*$, $v_r(10r_*)$ and flow opening angle, ω .

PSD found that radiatively driven winds from disks fall into two categories: 1) intrinsically unsteady with large fluctuations in density and velocity, and 2) steady with smooth density and velocity distributions. Which type of flow is produced depends on the geometry of the radiation field, parameterised by x : the flow is unsteady if the radiation field is dominated by the disk ($x < 1$), and steady if dominated by the star ($x \gtrsim 1$). The geometry of the radiation field also controls the geometry of the flow; the wind becoming more polar as x decreases. On the other hand, the mass-loss rate and terminal velocity are insensitive to geometry and depend more on the system luminosity, $L_D + L_*$.

Figure 1 compares the density in the wind in two models computed using the method of PSD (top panels), the full-Q formalism described here but setting the velocity gradient tensor elements which depend on the rotational velocity to zero (middle panels), and the full-Q formalism retaining all terms (bottom panels). The calculations in which $e_{r\phi}$ and $e_{\theta\phi}$ are set to zero (middle panels) are designed to test the effect of terms related to shear in the rotational velocity. At the same time, this removes the azimuthal force term altogether. The left column shows the results for a model in which $\dot{M}_a = 10^{-8} M_\odot \text{ yr}^{-1}$ and $x = 0$, the right column corresponds to $\dot{M}_a = \pi \times 10^{-8} M_\odot \text{ yr}^{-1}$ and $x = 3$. The former corresponds to the fiducial unsteady wind model discussed in detail in PSD. The latter gives a steady wind in which the force multiplier is well below M_{max} and hence should be strongly sensitive to the velocity gradient tensor representation.

First, we consider the changes seen in the $x = 0$ wind model (left-hand panels). This model remains unsteady in all three treatments of the line force. Details of the properties of the wind are changed, however. For example, the opening angle is increased from 42° to 50° between the PSD (top) and full-Q (bottom) results. In Table 1, it may be seen that the mass-loss rate increases by ~ 20 per cent between these two cases, while the characteristic velocity is the same. On the smaller scale of the flow substructure, we do find some subtle differences. Most notably, the slow, dense, complex portion of the wind extends further above the disk plane with full-Q case as compared in PSD.

In the steady wind models (right hand panels of Figure 1), similar fractional changes in the mass-loss rate are observed between the PSD and full-Q formulations and, again, the characteristic flow speeds are much the same. The main

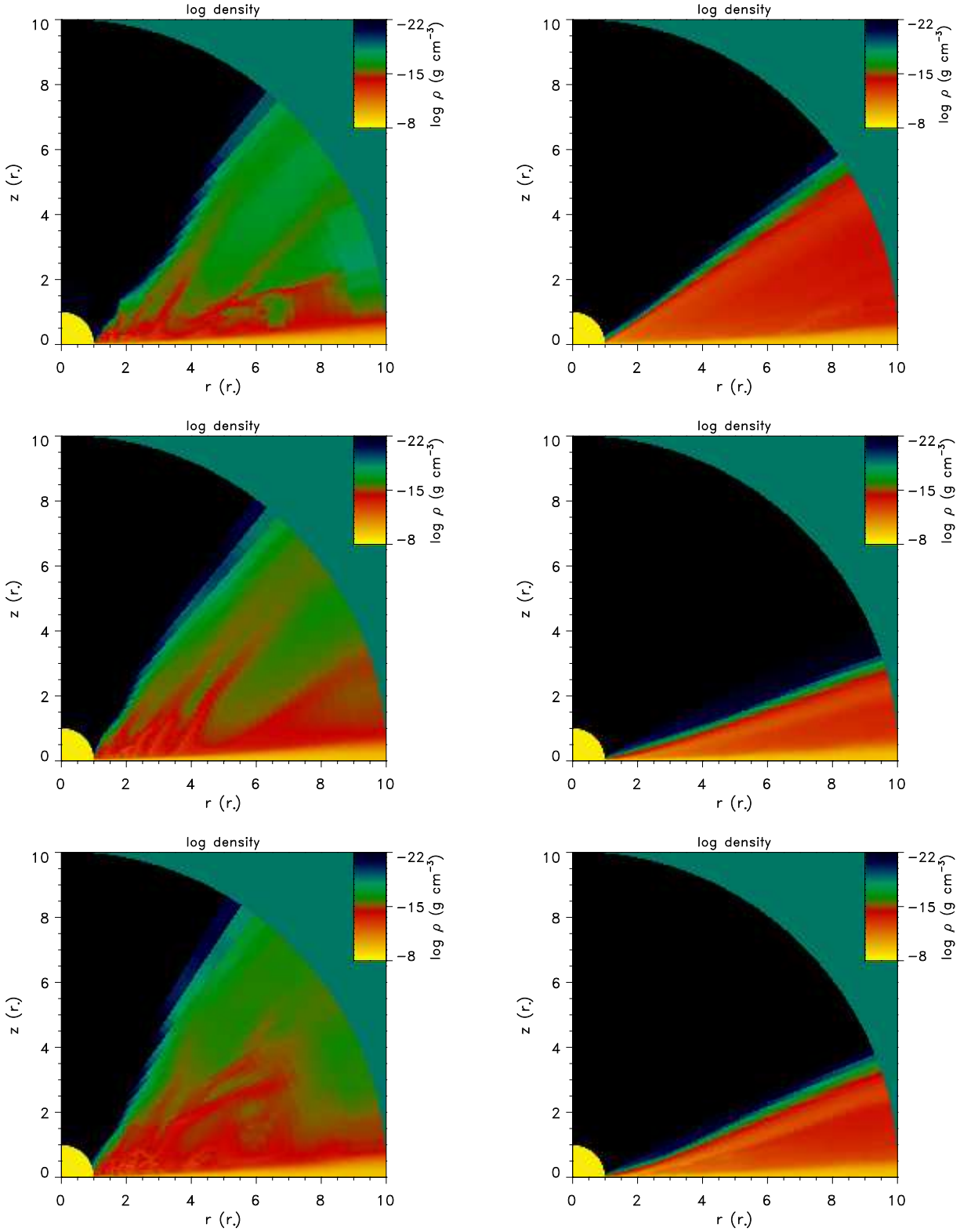


Figure 1. The density maps in two models computed using the method of PSD (top panels), the full-Q method but with $e_{r\phi} = e_{\theta\phi} = 0$ (middle panels), and the full-Q method retaining all terms (bottom panels). The left column shows the results for the unsteady model A while the right column shows results for the steady model D (see table 1, and section 4.1 for discussion).

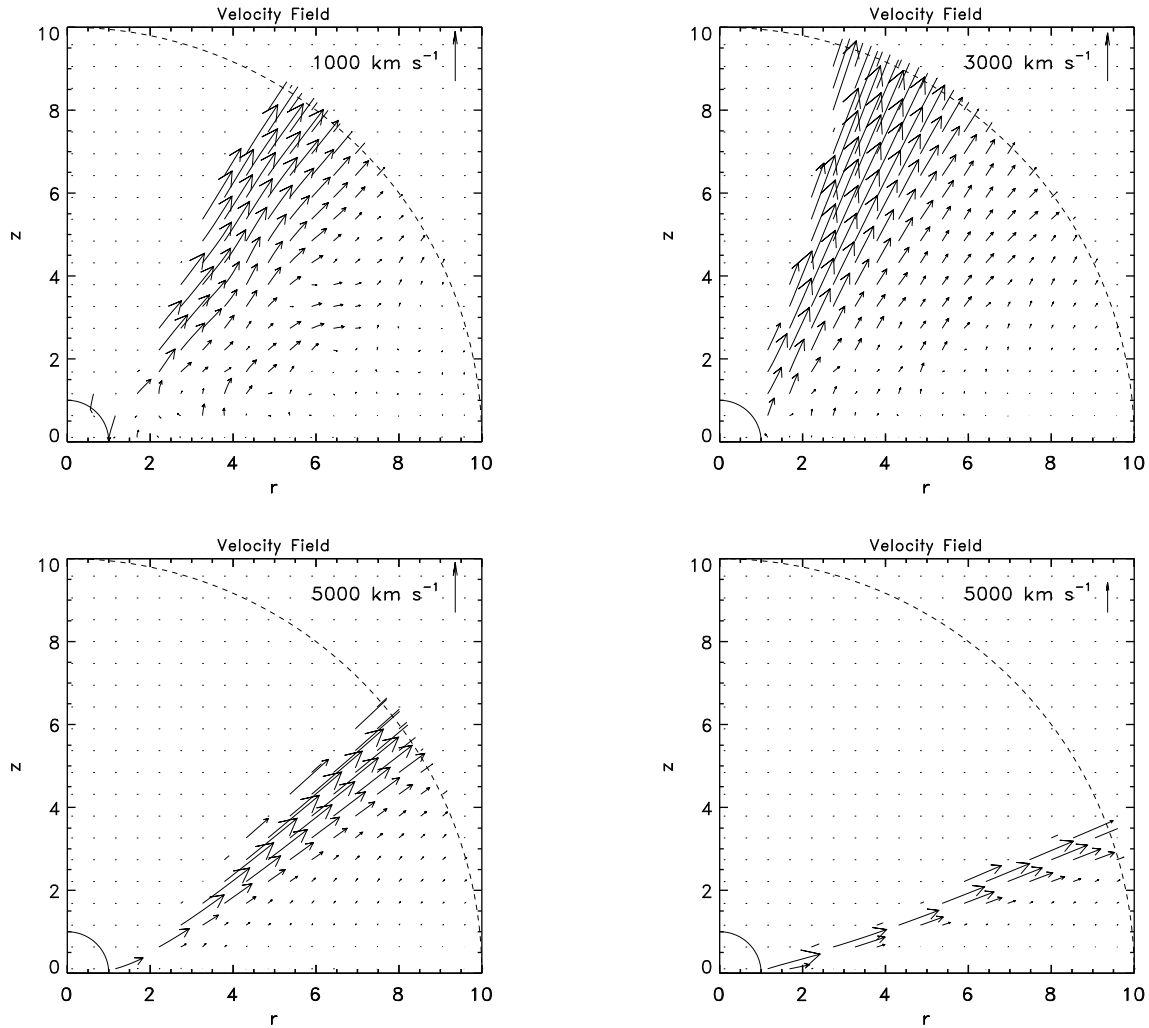


Figure 2. Maps of poloidal velocity for a range of models. The top two panels, a and b, are both models with $x = 0$ but with $\dot{M}_a = 10^{-8} M_{\odot} \text{ yr}^{-1}$ (model A) and $\dot{M}_a = \pi \times 10^{-8} M_{\odot} \text{ yr}^{-1}$ (model B), respectively. The bottom two panels, c and d, are results for models both with $\dot{M}_a = \pi \times 10^{-8} M_{\odot} \text{ yr}^{-1}$, but with $x = 1$ (model C) and $x = 3$ (model D). The top two panels show the effect on the outflow geometry of increasing the disk luminosity alone, while the top right and bottom two panels show the effect of adding in an increasingly larger stellar component ($x = 0, 1$ and 3) to the radiation field. Adding in an increasingly large stellar component causes the outflow to become more equatorial. Note that we suppress velocity vectors in regions of very low density (i.e., ρ less than $10^{-20} \text{ g cm}^{-3}$). The choice of input parameters for the models shown is the same as in Figure 10 of PSD.

difference is in the wind opening angle: in the full-Q case, the opening angle is distinctly smaller than in PSD. This is because the latitudinal component of the stellar line force gains more from the inclusion of the extra terms than either the radial component, or any of the disk contributions. The effect is stronger here than it happens to be in the unsteady wind models illustrated because the higher total luminosity of the system ensures that the general level of the force multiplier remains below saturation (i.e., $M(t) \lesssim 0.5 M_{\max}$).

In both the steady and unsteady wind models, the impact of the rotational shear terms is not very significant. The comparison between the middle and lower panels of Figure 1 reveals that the inclusion of these terms slightly increases the flow opening angle. We examined the origins of

this and found that this change is due to enhancing various components of the line force mainly in the inner disk.

In summary, our finding that the mass-loss rate and velocity are similar in the approximate PSD and full-Q cases can be explained by the fact that the terms in the velocity gradient tensor used by PSD are indeed dominant.

4.2 Overview of trends in the full-Q models

Figure 2 plots the poloidal velocity in four models computed with the full-Q method. Panels a and b compare the flow pattern from two models, with $x = 0$ in which the

Table 1. Summary of results for disc winds with $\alpha = 0.6$, $k = 0.2$, and $M_{max} = 4400$.

run	\dot{M}_a (M_\odot yr $^{-1}$)	x	\dot{M}_D (M_\odot yr $^{-1}$)	$v_r(10r_*)$ (km s $^{-1}$)	ω degrees
our					
A	10^{-8}	0	5.5×10^{-14}	900	50
B	$\pi \times 10^{-8}$	0	4.0×10^{-12}	3500	60
C	$\pi \times 10^{-8}$	1	2.1×10^{-11}	3500	32
D	$\pi \times 10^{-8}$	3	7.1×10^{-11}	5000	16
E	$\pi \times 10^{-8}$	10	3.2×10^{-10}	7000	8
PSD's					
2	10^{-8}	0	4.8×10^{-14}	900	42
3	$\pi \times 10^{-8}$	0	4.7×10^{-12}	3500	55
8	$\pi \times 10^{-8}$	1	2.1×10^{-11} ^(a)	3500	37
12	$\pi \times 10^{-8}$	3	6.3×10^{-11} ^(b)	5000	28
14	$\pi \times 10^{-8}$	10	3.1×10^{-10}	7000	24

a) We found a typographical error in PSD table 2 b) We calculated this model for longer than PSD did and we found that the flow settles at a higher mass-loss rate.

mass accretion rate and hence the disk luminosity L_D is increased: specifically, \dot{M}_a is raised from $10^{-8}M_\odot$ yr $^{-1}$ to $\pi \times 10^{-8}M_\odot$ yr $^{-1}$. By contrast, panels b, c, and d compare the flow pattern from three models in which the mass accretion rate is held fixed at $\dot{M}_a = 10^{-8}M_\odot$ yr $^{-1}$ while the stellar luminosity is varied using, $x = 0, 1$, and 3 . This diagram presents models with the same input parameters as those shown in Figure 10 in PSD, with the difference that here full-Q is implemented in their calculation and we plot poloidal velocity vectors instead of density.

Our new models confirm PSD's result that the flow becomes more equatorial as the contribution of the central star to the radiation field increases. However the scale of the changes in the flow geometry is greater for the full-Q case than in the approximate Q case – the models for low x are more polar here than in PSD, whereas the models for high x are more equatorial. PSD found that the reduction of the opening angle of the disk wind slows appreciably for $x \gtrsim 3$. With full-Q, this slowing is deferred until $x \gtrsim 5$. For example, we calculated the model for $x = 10$ and found $\omega = 8^\circ$, rather than $\omega = 24^\circ$ for PSD's corresponding model, run 14. Despite this geometric change, the gross wind properties as listed in Table 1 are scarcely any different.

The two models illustrated in Figure 1 showed that the model presented in PSD remains unsteady when recalculated using full Q, and that the originally steady model is still steady. We can generalise this further in that we find no noticeable shift in the value of x ($= L_*/L_D$) at which the change from unsteady to steady occurs. This is a further respect, to add to the mass-loss rate and characteristic flow speed, in which the full-Q models continue to closely resemble PSD's models.

5 DISCUSSION AND SUMMARY

The efficient algorithm described here has allowed us to examine the effects of all terms in the velocity gradient tensor on the structure of line-driven winds from disks. We find that the qualitative features of such winds are not changed by the more accurate algorithm used here. In particular, models which displayed unsteady behavior in PSD are also unsteady with the full-Q method. This indicates the approximations adopted in PSD indeed captured the dominant terms in the line force.

On generalizing the line force, we determine the geometry and strength of the line force in an exact way for a constant geometry of the radiation field. We continue to find, as in PSD, that the mass-loss rate and characteristic velocity do not depend on either of these two geometries but primarily on the total system luminosity. This is in keeping with the conclusion reached by Proga (1999) who showed that the mass-loss rate of even a simple spherically-symmetric stellar wind is of the same order of magnitude as that of a pure disk wind of the same total luminosity.

The dependence of the disk mass-loss rate on the total system luminosity, $L_D + L_*$, indicates that the irradiation due to the central star can power disk mass loss as does the disk radiation. Indeed we have already shown that the radiation from the luminous central star can drive a wind from an optically-thick disk of negligible intrinsic luminosity, i.e., for $x = 300$ and $L_D M_{max} \ll L_{Edd}$, where $L_{Edd} = 4\pi GM_*/\sigma_e$ is the Eddington luminosity (Drew, Proga & Stone 1998). The significance of irradiation has also been studied by Gayley, Owocki & Cranmer (1999). They also find, on the basis of a quite different formulation of the problem for an irradiated planar slab atmosphere, that the irradiation enhances or even induces the mass loss.

Whilst the radiation field geometry typically controls the geometry of the flow in the way described here and in PSD, there is a complicating effect that comes into play at low luminosities that has so far gone unremarked. When $L_D M_{max} \lesssim$ a few L_{Edd} , we find that the upper bound, M_{max} on the force multiplier exerts an influence on the geometry of the disk wind. In particular for $x = 0$, our models show that the higher M_{max} , the higher the wind opening angle becomes. Proga (1999) calculated a few models for $x = 0$ without saturation of $M(t)$ (his models in the CAK&FD case) and found that $\omega \approx 90^\circ$ regardless of disk luminosity. Calculation using our full-Q method confirm this result.

The changes caused by the full-Q treatment in disk winds are not so serious as in winds around rapidly rotating oblate stars. OCG's treatment of the rotating stellar wind case was a big step forward in that their inclusion of all terms in Q introduced latitudinal and azimuthal components of the line force where, before, only the radial component had been considered. They found that (i) the latitudinal component is poleward and unopposed by any other force and hence is dynamically significant in inhibiting the equatorward drift of the wind; (ii) the azimuthal line force acts against the sense of rotation and is less significant because it causes only a modest spin-down of the wind rotation. In the disk wind case, however, there is only one qualitative change with respect to our own earlier treatment (PSD) when all Q terms are included: there is now a non-zero azimuthal line force. Again, as in the rotating stellar wind case, this is rather weak as compared to the other components and is not of great importance. The importance of this azimuthal term is further weakened by the fact that it can spin-down or spin-up the wind rotation depending on location and time. Its sign may change in disk winds because the wind velocity field is complex and so the contribution of all Q terms symmetric in ϕ can be positive or negative (even dv_r/dr is negative in some regions of disk winds).

The fact that the unsteady behavior observed in our models has not changed with a more accurate treatment of the radiation force indicates it is indeed a robust property of line driven winds from disks. Why does increasing the radial component of the radiation force 'organize' the wind into a steady state? Let r' and z' define position along a streamline in the wind in cylindrical coordinates. An increase of the vertical component of the gravity,

$$g_z \propto -\frac{z'}{(r'^2 + z'^2)^{3/2}} \quad (18)$$

with height at a fixed radius r' is the main driver of the unsteady flow. However this increase of the gravity can be significantly reduced if the streamlines are directed outwards from purely vertical (i.e., r' increases with z'). At the same time, this tilt also brings into play an increase of the horizontal effective gravity, g_r , along each streamline:

$$g_r \propto \frac{r_f}{r'^3} - \frac{r'}{(r'^2 + z'^2)^{3/2}}, \quad (19)$$

where r_f is the radius on a Keplerian disk at which a streamline originates. However the increase of g_r with r' is slower than the increase of g_z with z' because of the decaying centrifugal term. In other words, the line force can more easily maintain domination over gravity if the flow climbs the gentler gravitational hill in the horizontal direction as compared with the vertical direction. Furthermore, driving material along streamlines outward from the vertical causes density to decline as $1/r'$ as required by geometrical dilution – this, very usefully, tends towards increasing the line force, thereby facilitating a better match with trends in gravity.

Despite our progress in developing realistic models for line-driven disk winds, limitations obviously remain. For example we calculate the line-force using the Sobolev approximation. It is questionable if this approximation is valid in cases where the wind is slow and/or highly structured. Even if the Sobolev approximation is locally valid in those cases, our full-Q method does not account for non-local effects in line transfer. For example, our line force is potentially overestimated in upper parts of the flow because of neglect of self-shadowing. Our models also assume axisymmetry – in particular that the disk plane is flat and perpendicular to the rotational axis whereas in reality disks may be tilted or twisted. We also simplify the thermal structure of the disk wind by assuming that it is isothermal. In our models, the disk is not isothermal to start with, and we need also to calculate of the ionization structure and energy balance to properly model the wind thermodynamics and the radiation pressure.

Another aspect of our models to date that will need to be revisited in future is the prescription for the reemission of disk irradiation. We have assumed thus far that the disk re-emits all absorbed energy locally and isotropically. Gayley et al. (1999) have opted for more or less the opposite prescription appropriate to purely scattering atmospheres. Strictly, detailed NLTE photoionization calculations of externally-irradiated disks need to be performed on a case-by-case basis as it is not obvious a priori what prescription should be used in any one situation.

Models of line-driven winds from luminous disks show promise of being able to explain mass loss phenomena associated with e.g., cataclysmic variables, massive young stellar objects and extreme Be objects (e.g., PSD, Drew, Proga & Stone 1998, Oudmaijer et al. 1998). Our further progress in understanding those winds requires a direct, quantitative comparison between observations and model predictions. Therefore we plan to use our three-dimensional disk wind structure to calculate synthetic line profiles – initial work is underway. We also plan to further develop our disk wind models. For example, we intend to calculate the photoionization structure of the wind that will allow to take into account changes of the line force with local ionization. With such improvements our models will be readily applicable to the systems with a very wide dynamical range such as AGN. An outcome of the present study has been to confirm the unsteady behaviour in predominantly disk-illuminated models, first identified in the more approximate calculations due to PSD. To test this, we have obtained an allocation of

Hubble Space Telescope time to carry out a high time- and spectral-resolution study of 3 nova-like variables – objects in which we expect disk winds to be driven primarily by disk radiation. If winds in these systems are unsteady then we hope to see evidence of this in the form of time-variable fine structure in blueshifted absorption features.

Acknowledgments: This research has been supported by a research grant from PPARC. Computations were performed at the Imperial College Parallel Computing Centre.

REFERENCES

Batchelor G.K. 1967, An Introduction to Fluid Mechanics (Cambridge: Cambridge University Press)

Castor J.I., Abbott D.C., Klein R.I., 1975, ApJ, 195, 157 (CAK)

Drew J.E., Proga D., Stone J.M., 1998, MNRAS, 296, L6

Friend D.B., Abbott D.C., 1986, ApJ, 311, 701

Gayley K.G., Owocki, S.P., Cranmer, S.R. 1999, ApJ, 513, 442

Icke V., 1980, AJ, 85, 329

Murray N., Chiang J., Grossman S.A. Voit, G.M., 1995, ApJ, 451, 498

Oudmaijer R. D., Proga D., Drew J. E., de Winter D., 1998, MNRAS, 300, 170

Owocki S.P., Castor J.I., Rybicki, G.B. 1988, ApJ, 335, 914

Owocki, S.P., Cranmer, S.R., Gayley K.G. 1996, ApJ, 472, L115 (OCG)

Pauldrach A., Puls J., Kudritzki R.P., 1986, A&A, 164, 86

Pereyra N.A., Kallman T.R., Blondin J.M., 1997, ApJ, 477, 368

Proga D. 1999, MNRAS, 304, 938

Proga D., Stone J.M., Drew J.E., 1998, MNRAS, 295, 595 (PSD)

Rybicki G.B., Hummer D.G. 1978, ApJ, 219, 654

Shakura N.I., Sunyaev R.A. 1973 A&A, 24, 337

Stone J.M., Norman M.L. 1992, ApJS, 80, 753

Vitello P.A.J., Shlosman I., 1988, ApJ, 327, 680